A Framework for Ice Sheet - Ocean Coupling (FISOC) V1.1

Rupert Gladstone[1], Benjamin Galton-Fenzi[2], David Gwyther[3], Qin Zhou[4], Tore Hattermann[5,10], Chen Zhao[3], Lenneke Jong[2], Yuwei Xia[6], Xiaoran Guo[6], Konstantinos Petrakopoulos[8], Thomas Zwinger[9], Daniel Shapero[7], and John Moore[1,6]

[1]Arctic Centre, University of Lapland, Rovaniemi, Finland
[2]Australian Antarctic Division
[3]University of Tasmania, Hobart, Australia
[4]Akvaplan-niva AS, Tromsø, Norway
[5]Norwegian Polar Institute, Tromsø Norway
[6]Beijing Normal University, China
[7]University of Washington, Seattle, US
[8]Center for Global Sea Level Change, New York University Abu Dhabi, United Arab Emirates
[9]CSC IT Center for Science, Espoo, Finland
[10]Energy and Climate Group, Department of Physics and Technology, The Arctic University - University of Tromsø, Norway

Correspondence: Rupert Gladstone
(RupertGladstone1972@gmail.com)

Abstract.

A number of important questions concern processes at the margins of ice sheets where multiple components of the Earth System, most crucially ice sheets and oceans, interact. Such processes include thermodynamic interaction at the ice-ocean interface, the impact of melt water on ice shelf cavity circulation, the impact of basal melting of ice shelves on grounded ice dynamics, and ocean controls on iceberg calving. These include fundamentally coupled processes in which feedback mecha-

5 nisms between ice and ocean play an important role. Some of these mechanisms have major implications for humanity, most notably the impact of retreating marine ice sheets on global sea level. In order to better quantify thesemechanisms using computer models, feedbacks need to be incorporated into the modelling system. To achieve this ocean and ice dynamic models must be coupled, allowing run time information sharing between components. We have developed a flexible coupling framework

10 based on existing Earth System coupling technologies. The open-source Framework for Ice Sheet – Ocean Coupling (FISOC) provides a modular approach to online coupling, facilitating switching between different ice dynamic and ocean components. FISOC allows fully synchronous coupling, in which both ice and ocean run on the same time-step, or semi-synchronous coupling in which the ice dynamic model uses a longer time step. Multiple regridding options are available, and multiple methods for coupling the sub ice shelf cavity geometry. Thermodynamic coupling may also be activated. We present idealised simula-

15 tions using FISOC with a Stokes flow ice dynamic model coupled to a regional ocean model. We demonstrate the modularity of FISOC by switching between two different regional ocean models and presenting outputs for both. We demonstrate conservation of mass and other verification steps during evolution of an idealised coupled ice - ocean system, both with and without grounding line movement.

1 Introduction

20 The Antarctic and Greenland ice sheets have the potential to provide the greatest contributions to global sea level rise on century timescales (Church et al., 2013; Moore et al., 2013), with the greatest uncertainty in projections being due to the Marine Ice Sheet Instability (MISI) (Mercer, 1978; Schoof, 2007; Robel et al., 2019). Ice dynamic behaviour is strongly sensitive to ocean currents, in particular the transport of warmer waters across the continental shelf causing high basal melt rates under ice shelves (Hellmer et al., 2012; Thoma et al., 2015). For Antarctica's Pine Island Glacier, which is likely undergoing unstable
25 retreat due to MISI, ocean induced basal melting has been established as a trigger for MISI through both observational evidence (Christianson et al., 2016) and model studies (Favier et al., 2014; Gladstone et al., 2012). While MISI is fundamenatally a geometrically controlled phenomenon, its onset and the resulting rate of ice mass loss are strongly dependent on tight coupling between ice dynamic behaviour and ocean processes. Importantly, ocean-driven basal melt rates respond to the evolving geometry of ice shelf cavities (Mueller et al., 2018), and the grounded-ice dynamic behaviour responds to the evolving basal
30 melt rates through their impact on the buttressing force provided by ice shelves to the grounded ice. While most ice sheet model based studies use relatively simple parameterisations for calculating basal melt rates beneath ice shelves, a recent comparison has highlighted limitations of this approach (Favier et al., 2019). In particular, melt parameterisations as a function of depth or thermal driving do not impose conservation of heat in the system, and none of the parameterisations fully capture the impact of evolving ice geometry on cavity circulation.

35 Several projects to couple ice sheet and ocean models are underway, and most (including the current study) will contribute to the Marine Ice Sheet – Ocean Model Intercomparison Project first phase (MISOMIP1) and its child projects: the Marine Ice Sheet Model Intercomparison Project third phase (MISMIP+); and the Ice Shelf Ocean Model Intercomparison Project second phase (ISOMIP+) (Asay-Davis et al., 2016).

Coupling projects take different approaches to handling the different timescales of ice and ocean processes. An ice sheet
40 flowline model coupled to a five box ocean model allows large ensemble simulations to be carried out, but is limited in terms of implementation of physical processes (Gladstone et al., 2012). A temporally synchronous approach allows the cavity geometry to evolve on the ocean time-step as a function of the melt rates calculated by the ocean model and the ice dynamics calculated by the ice model (Goldberg et al., 2018). Asynchronous approaches incorporate a longer time-step for ice than ocean, and sometimes involve offline coupling with partial restarts for the ocean model (Seroussi et al., 2017; De Rydt and Gudmundsson,
45 2016; Thoma et al., 2015).

Here we present a new flexible Framework for Ice Sheet – Ocean Coupling (FISOC, Section 2). FISOC allows runtime coupling between ice and ocean components with a user choice of synchronicity options. Adopting Earth System Modelling Framework terminology (ESMF; Section 2), we refer to an ocean model coupled through FISOC as an "ocean component" and an ice sheet or ice dynamic model coupled through FISOC as an "ice component". We use FISOC to couple two different
50 3D ocean models to an ice dynamic model and present idealised simulations demonstrating mass conservation and consistent grounding line behaviour (Section 3). FISOC is also currently being used to contribute to ISOMIP+ and MISOMIP1.

2 Methodology

FISOC is an open source coupling framework built using the Earth System Modelling Framework (ESMF, Hill et al. (2004); Collins et al. (2005)). FISOC aims to provide seamless runtime coupling between an existing ice sheet model and an existing ocean model for application to Antarctic ice sheet - ocean systems. In its current form, FISOC assumes that the important ice sheet - ocean interactions occur at the underside of a floating ice shelf, and that the lower surface of the ice shelf can be projected on to the horizontal plane.

FISOC aims to provide flexibility and computational efficiency through the following key features:

– Flexible modular architecture (Section 2.1) facilitates swapping between different ice components or between different ocean components according to purpose (Section 2.2).

– Access to ESMF tools allows multiple regridding and interpolation options, including between regular grids and unstructured meshes (Section 2.3).

– Multiple options for handling differing ice and ocean time scales include fully synchronous coupling, passing rates of change, time averaging of variables (Sections 2.4 and 2.5).

– Flexible run-time control over the exchange of variables allows specific coupling modes to be (de)activated as required, e.g. geometric coupling, thermodynamic coupling.

– Grounding line movement (Section 2.8) is implemented using geometry change rates and a modified wet/dry scheme in the ocean component, with multiple options available for updating cavity geometry (Section 2.5).

– Flexibility for parallelisation options. Currently sequential coupling is implemented, but any combination of sequential and concurrent parallelisation is possible with minimal coding effort.

– ESMF compatibility means that FISOC can be embedded within any ESMF-based modelling system, e.g. as a regional model within a global model.

– ESMF compatibility also means that additional ESMF components (e.g. an atmosphere model) could easily be added to the coupled system.

These features are described further in the following sections and in the FISOC manual, which can be found in the FISOC repository (see "code availability" at the end of this paper).

2.1 Software design

While coupled models in Earth System science have been in existence for decades, and such coupled models are often viewed as single entities (ocean - atmosphere general circulation models for example), the field of coupled ice sheet - ocean modelling is relatively young. FISOC is intended as a framework for coupling independent models rather than as a coupled model in itself. Building and running a coupled ice sheet - ocean model is currently more complex than building and running both an ice and an ocean model independently. FISOC aims to minimise the additional complexity.
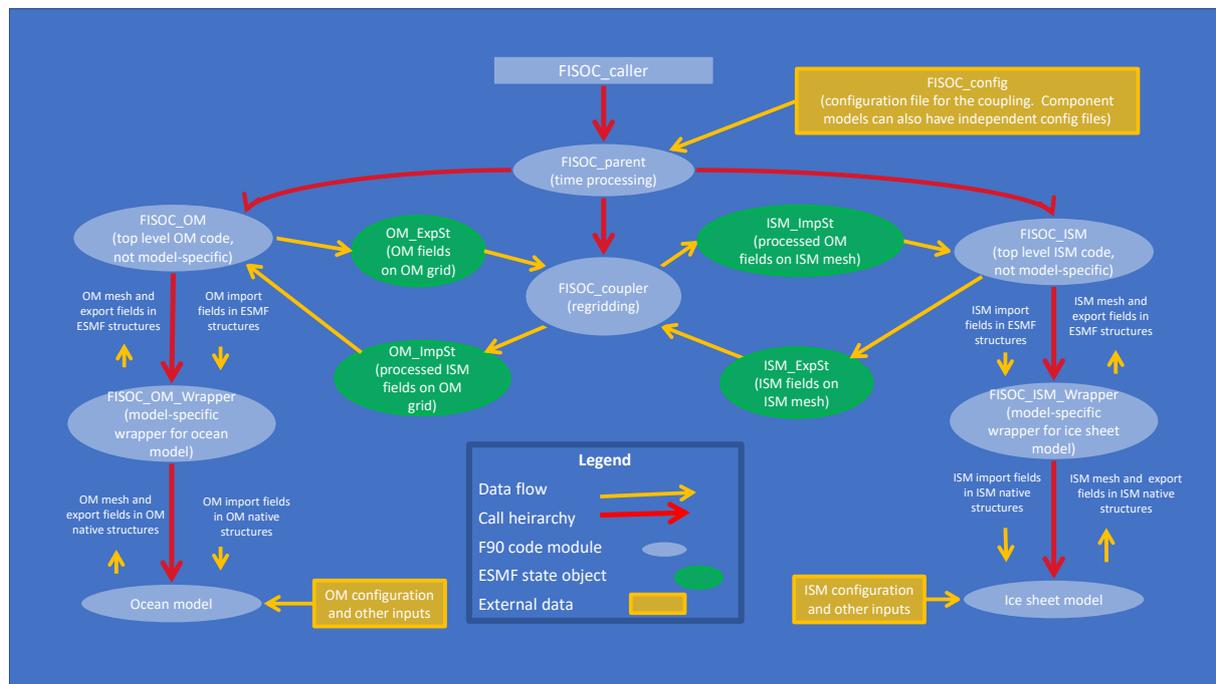
Figure 1. Overview of FISOC code structures. "OM" and "ISM" are short for Ocean and Ice Sheet Model respectively. "ImpSt" and "ExpSt" are short for Import and Export State respectively.

The ice and ocean components may use their standard run time input files, and their paths are set in a FISOC run time configuration file, along with information about time-stepping and variables to be exchanged.

85 FISOC adopts the hierarchical modular structure of the Earth System Modelling Framework (ESMF, Hill et al. (2004); Collins et al. (2005)). The FISOC code structures are summarised in Figure 1. A top level executable calls a FISOC parent module (this could in principal also be embedded within a larger coupled model framework). The parent module coordinates calling of the ice, ocean and regridding components. Regridding is one of the reasons to make use of ESMF, described further in Section 2.3. The ice and ocean components are independent models, not included in the FISOC code repository, compiled

90 as libraries to be called by FISOC at run time. On each side (ice and ocean) of the coupling is a model-specific wrapper, whose main run time functions are:

- Call the component's initialise, run and finalise routines as required.

- Convert the component's grid or mesh to ESMF format, using ESMF data structures.

- Read from, or write to, the component's required state variables, converting between the component's native data struc-
95 tures and ESMF data structures.

Further processing of variables (such as calculating rates of change) is implemented by the ice and ocean generic code modules.

Incorporating a new ice or ocean component into FISOC can be straightforward, depending on the existing level of ESMF compatibility of the new component. Models able to provide mesh information and variables in ESMF data structures can be

100 very easily built in to FISOC. The only coding required for a new component is a new model-specific wrapper in the FISOC repository. Copying an existing wrapper can be a viable starting point.

2.1.1 Error handling

The ESMF adopts a defensive strategy to error handling: All errors are logged and passed back up the call stack. The calling routine has the option of attempting to continue running in the event of errors occurring. As the call structure between FISOC

105 and ESMF is one-way (FISOC routines may call ESMF routines but not vice versa) all such errors are eventually returned to FISOC.

FISOC adopts a fail-fast approach. Errors are generally considered to be fatal, in which case FISOC will log error information and finalise both ice and ocean components and ESMF. FISOC also aims to provide consistency checks, most of which are considered fatal if not passed. For example, ice and ocean input files might both contain time-stepping information, potentially

110 duplicating information in the FISOC run-time configuration file, and these can be checked for consistency in the model-specific wrappers. The general intention is to stop running if something unexpected happens and provide a meaningful message to the user about why.

There are a few cases where ESMF errors can be handled at run time. Details can be found in the FISOC manual.

2.2 Components

115 FISOC is designed to facilitate swapping between different ocean or ice components. Currently two different ocean components and one ice component are available through FISOC. Table 1 summarises components currently coupled into FISOC. In some cases a non-standard build of the component is required for FISOC compatibility, and these are described in the FISOC manual, which can be obtained through the FISOC repository (Section 2.1).

The ice component Elmer/Ice (Gagliardini et al., 2013) is a powerful, flexible, state-of-the-art ice dynamic model.

120 The Regional Ocean Modelling System (ROMS; Shchepetkin and McWilliams (2005)) is a 3D terrain-following sigma coordinate ocean model that has already been adapted to use in ice shelf cavities (Galton-Fenzi et al., 2012). The module for ice shelf cavities implemented in the Finite Volume Community Ocean Model (FVCOM, Chen et al. (2003)) provides non-hydrostatic options, a horizontally unstructured mesh that lends itself to refinement, and may be more suited to small scale processes such as ice shelf channels (Zhou and Hattermann, 2020).

Table 1. Ice and ocean components currently coupled through FISOC.

Type	Name	Notes
OM	ROMS	3D, gridded, sigma coord
OM	FVCOM	3D, unstructured mesh, sigma coord
ISM	Elmer/Ice	3D, full Stokes and shallow models

2.3 Regridding

As stated above, FISOC provides coupling on a horizontal plane onto which the lower surface of an ice shelf can be projected. It is this plane on which ice and ocean properties are exchanged through the FISOC framework. Adapting the FISOC code to handle a vertical ice cliff is expected to be straightforward, and would be desirable for application to the Greenland ice sheet. More complex 3D ice-ocean interface geometries are challenging not only for FISOC but also for the current generation of ice sheet and ocean models.

FISOC has access to all the run-time regridding options provided by ESMF. These include nearest neighbour options, conservative options, patch recovery and bilinear regridding. These options are available for structured grids and unstructured meshes. FISOC requires that both ice and ocean components define their grid or mesh on the same coordinate system, and that both components use the same projection. All FISOC simulations to date have used a Cartesian coordinate system.

When using FISOC to couple Elmer/Ice to ROMS, the ROMS staggered grid, including ghost cells, extends beyond the domain of the Elmer/Ice mesh. ESMF regridding methods also provide options for extrapolation which are used here. Simulations in the current study use either nearest "Source TO Destination" (STOD, a form of nearest neighbour regridding) or use bilinear interpolation with nearest STOD to extrapolate to points outside the domain.

2.4 Coupling timescales

The timescales for sub-shelf cavity circulation behaviour are in general much shorter than the timescales for ice flow and geometry evolution (typically minutes to days instead of years to centuries). Typical time-step sizes are correspondingly smaller for ocean models (seconds to minutes) than for ice sheet models (days to months). A single ice sheet model time-step, if the Stokes equations are solved in full, will typically require orders of magnitude more computational time than a single ocean time-step. Due to the combination of these two reasons the ice and ocean components of FISOC will in general use different time-steps, with the ice time-step being much larger. We define relevant terminology for coupling timescales:

– **Fully synchronous coupling.** The ice and ocean components have the same time-step size, and exchange variables every time-step.

- **Semi synchronous coupling.** The ice component has a larger time-step than the ocean component, but cavity geometry and grounding line position are allowed to evolve on the ocean time-step (e.g. by using ice velocities from a previous ice time-step or rates of change based on the most recent two time-steps).

- **Asynchronous coupling.** The ice component has a larger time-step than the ocean component. Cavity geometry is updated on the ice component time-step or less frequently.

- **Coupling interval.** The time interval at which the ice and ocean components exchange variables.

FISOC requires the coupling interval to be an exact multiple of both the ocean time-step size and the ice component time-step size. FISOC assumes that time-step sizes are not adaptive. Simulations in the current study set the coupling interval equal to the ice component time-step size.

In principal, FISOC supports all three synchronicity options, though fully synchronous coupling is not practical to achieve when solving the Stokes equations for the ice. The experiments carried out for this paper use semi synchronous coupling with cavity geometry evolution as described in Section 2.5.

Goldberg et al. (2018) and Snow et al. (2017) implement fully synchronous coupling, whereas Seroussi et al. (2017) and Favier et al. (2019) implement asynchronous coupling with partial ocean restarts.

2.5 Handling cavity evolution

The evolution of cavity geometry under the ice shelf, defined by ice draft and grounding line location, is calculated by the ice component using the melt rates passed from the ocean component. But the ocean and ice components are typically run on different grids/meshes, and both components need to maintain a representation of the ice draft and grounding line position on their native grid or mesh. Information about the ice component cavity evolution must be passed to the ocean component.

Given the potential for non-synchronicity of the ice and ocean component time-stepping, several methods are implemented in FISOC for the ocean to update its representation of the ice draft. All the processing options described below are applied on the ocean grid after the ice component representation of ice geometry has been regridded. We use subscripts with square brackets, $_{[X]}$, where X is either O (ocean component) or I (ice component), to denote a variable that exists in both ice and ocean components with the same physical meaning, but potentially different values due to being represented on different grids/meshes.

Most recent ice. The simplest option is that the ocean component uses the ice draft directly from the most recent ice component time-step. If fully synchronous coupling is used this option should be chosen. The main disadvantage of this approach for semi or asynchronous coupling is that, due to the much longer time-step of the ice component, the ocean component will experience large occasional changes in ice draft instead of smoothly evolving ice draft. This could be both physically unrealistic and potentially numerically challenging for the ocean component.

Rate. The vertical rate of change of ice draft is calculated by FISOC from the two most recent ice component time-steps:

$$\frac{dD_{[O,t]}}{dt} = \left(D_{[I,t]} - D_{[I,t-\Delta t_i]} \right) / \Delta t_I \tag{1}$$

180   where $D_{[O,t]}$ is the ocean component's representation of ice draft at time t, $D_{[I,t]}$ is the ice component's representation of ice draft at time t, $D_{[I,t-\Delta t_I]}$ is the ice component's representation of ice draft at time $t-\Delta t_I$, and Δt_I is the ice component time-step size. This rate of change is used by the ocean component to update the cavity geometry. This approach provides temporally smooth changes to the ocean representation of the ice draft, but has the potential for the ice and ocean representations to diverge over time as a result of regridding artefacts.

185   **Corrected rate**. The same as above, except that a drift correction is applied to ensure ice and ocean representations of cavity geometry do not diverge.

$$\frac{dD_{[O,t]}}{dt} = \frac{D_{[I,t]} - D_{[I,t-\Delta t_I]} + f_{cav}\left(D_{[I,t]} - D_{[O,t]}\right)}{\Delta t_I} \tag{2}$$

where f_{cav} is a cavity correction factor between 0 and 1. Equation 2 is applied at coupling time-steps, and the calculated rate of cavity change is then held constant during ocean component evolution until the next coupling time-step.

190   **Linear interpolation**. The ocean representation of the ice draft is given by temporal linear interpolation between the two most recent ice sheet time-steps. This imposes additional lag of the ocean component behind the ice component.

The above options are all implemented in FISOC, but only the "rate" and "corrected rate" approaches are used in the current study.

The cavity geometry may be initialised independently by ice and ocean components. In this case the user must ensure
195   consistency. It is also possible for the cavity geometry from the ice component to be imposed on the ocean component during FISOC initialisation. This ensures consistency.

Handling cavity evolution is a little more complicated in the case of an evolving grounding line, as discussed in Section 2.8 below.

2.6   Thermodynamics at the ice-ocean interface

200   Exchange of heat at the ice-ocean interface is handled within the ocean model. Like many ocean models, FVCOM and ROMS adopt the three-equation formulation for thermodynamic exchange (Hellmer and Olbers, 1989; Holland and Jenkins, 1999). This parameterisation assumes that the interface is at the in situ pressure freezing point, and that there is a heat balance and salt balance at the interface. An ablation or melt rate is calculated for each ocean model grid cell, which is then passed to FISOC as a boundary condition for the lower surface of the ice model at the coupling time interval.

205   Internally, both ocean models account for the thermodynamic effect of basal melting by imposing virtual heat and salt fluxes within a fixed geometry at each ocean model time step, to mimic the effects of basal melting, rather than employing an explicit volume flux at the ice-ocean interface. Independent of this, a geometry change is passed back from the ice model through FISOC at the coupling time step (including the effect of melting/freezing, as well as any ice dynamical response), which is used to update the ocean model ice shelf cavity shape (Section 2.5).

210   For some applications, conductive heat fluxes into the ice shelf due to vertical temperature gradients in the ice at the ice-ocean interface are required by the three-equation parameterisation to calculate the flux balance at the ice ocean interface. While ice-ocean thermodynamic parameterisations in ocean-only models must make an assumption about this temperature

gradient, FISOC can pass the temperature gradient from the ice component directly to the ocean component. This feature is not demonstrated in the current study, but will be properly tested in future studies.

2.7 Interface pressure

Aside from the geometry evolution, an ocean boundary condition for pressure at the ice-ocean interface, $P_{interface}$, must be provided to the ocean component. FISOC can pass pressure directly from ice to ocean components. However, using actual ice overburden directly as an upper ocean boundary condition results in higher horizontal pressure gradients at the grounding line (and for dry cells, see Section 2.8) than ocean models can typically handle (Goldberg et al., 2018). In the current study, the ocean component uses ice draft (i.e. the depth of the ice-ocean interface) to estimate a floation pressure. ROMS assumes a constant reference ocean density:

$$P_{interface} = g\rho_{or}D_{[O]} \tag{3}$$

where g is acceleration due to gravity, ρ_{or} is a reference ocean density and $D_{[O]}$ is the ocean representation of ice draft. For the current study, all simulations with ROMS use $\rho_{or} = 1027\,\mathrm{kg\,m^{-3}}$. FVCOM assumes a constant vertical ocean density gradient following Dinniman et al. (2007):

$$P_{interface} = g(\rho_{o1} - 0.5\frac{d\rho_o}{dz}D_{[O]})D_{[O]} \tag{4}$$

where ρ_o is ocean water density, ρ_{o1} is ocean water density of the top ocean layer and the vertical ocean water density gradient, $\frac{d\rho_o}{dz}$, is set to $8.3927 \times 10^{-4}\mathrm{kgm^{-4}}$.

2.8 Grounding line evolution

Grounding line movement in FISOC requires that both ice and ocean components support it. Numerical convergence issues place constraints in terms of mesh resolution for representing grounding line movement in ice sheet models (Vieli and Payne, 2005; Pattyn et al., 2006; Gladstone et al., 2010a, b; Cornford et al., 2013; Gladstone et al., 2017). While FISOC allows ice draft to be passed to the ocean component (Section 2.5), FISOC does not impose the ice component grounding line position on the ocean component. Instead, the ocean component uses the evolving cavity geometry to evolve the grounding line.

A recent ice-ocean coupling study (Goldberg et al., 2018) used a "thin film" approach to allow grounding line movement. A thin passive water layer is allowed to exist under the grounded ice, and an activation criterion is imposed to allow the layer to inflate to represent grounding line retreat. The current study takes a conceptually similar approach, modifying the existing wetting and drying schemes independently in both ROMS (Warner et al., 2013) and FVCOM. "Dry" cells are used for the passive water column under grounded ice and "wet" cells are used for the active water column under floating ice or the open ocean. The wet - dry mask is two dimensional, so while it is conventional to talk about dry or wet cells, this actually refers to dry or wet columns. The grounding line evolves in the two horizontal dimensions, and is represented in the ocean component as the vertical surface between dry and wet columns.

The original criterion in both ROMS and FVCOM for a cell to remain dry is given by:

$$\eta - z_b < D_{crit} \tag{5}$$

245 where η is the free surface variable, z_b is the bottom boundary depth (bathymetry, aka bedrock depth), and D_{crit} is a critical water column thickness (or depth) for wet/dry activation. D_{crit} is a parameter to be set by the user (typical values lie between 1 to 20m). Both η and z_b are defined relative to sea level. Thus cells with a water column thickness less than D_{crit} are designated dry. Flux of water into dry cells is allowed, but flux of water out of dry cells is prevented.

The FVCOM criterion for an element to be dry has been modified for the presence of a marine ice sheet/shelf system as 250 follows:

$$\eta - z_b + D_{[O]} < D_{crit} \tag{6}$$

The ROMS criterion for a cell to be dry has been modified for the presence of a marine ice sheet/shelf system as follows:

$$\eta + z_b - (S_{[O]} - D_{[O]} + D_{crit}) * \frac{\rho_i}{\rho_{or}} \leq 0 \tag{7}$$

where $S_{[O]}$ is the ocean representation of ice sheet/shelf upper surface height and $D_{[O]}$ is the ocean representation of ice draft.

255 FISOC allows the ice component to pass any geometry variables to the ocean, such as ice draft, ice thickness, upper surface elevation, or rates of change of any of these. In the event that geometry variables other than D are passed to the ocean, the same processing method is used as for D, as described in Section 2.8.

In the current study $\frac{dD}{dt}$ is passed to the ocean component, and in one case both $\frac{dD}{dt}$ and $\frac{dS}{dt}$ are passed (details in Section 3). When $\frac{dS}{dt}$ is passed, $\frac{dS}{dt}$ is processed the same way as $\frac{dD}{dt}$.

260 If the grounding line problem is solved, and if D is processed for passing to the ocean using the **Corrected rate** method, equation 2 is modified to account for the dry water column thickness, which is initialised to D_{crit}. The correction term changes from $f_{cav}\left(D_{[I,t]} - D_{[O,t]}\right)$ to $f_{cav}\left(\max(D_{[I,t]}, zb + D_{crit}) - D_{[O,t]}\right)$.

3 Verification experiment design

Simulations are carried out on idealised domains as a proof of concept to demonstrate the coupling rather than to address 265 scientific questions. Verification experiment 1 (VE1) aims to assess whether the coupled system conserves mass. Verification experiment 2 (VE2) aims to assess whether the ocean and ice representations of grounding line evolution are consistent.

3.1 Verification experiment 1: Floating adjustment

Verification experiment 1 (VE1) is a simple experiment in which a linearly sloping ice shelf is allowed to adjust toward steady state. The experiment is not run long enough to attain steady state, but enough to demonstrate evolution of the coupled system. 270 See Table 2 for run length and a summary of other model choices and parameter values used in VE1.

All ice and ocean vertical side boundaries are closed: There is no flow in or out of the domain. There is mass exchange between the ice and ocean (and therefore also heat exchange). The coupling is purely geometric in that the ocean component

Table 2. Model choices and input parameters used in verification experiment 1 (VE1, Section 3.1) and verification experiment 2 (VE2, Section 3.2) comprising four simulations in total: VE1_ER, VE1_EF, VE2_ER and VE2_EF. Component abbreviations in these simulation names are E (Elmer/Ice), R (ROMS), and F (FVCOM). "Semi-structured" refers to a mesh that is in principal unstructured, but in practice structure can be seen (See Figure 2 middle and lower panes).

Choice or input	VE1_ER	VE1_EF	VE2_ER	VE2_EF
Ice component	Elmer/Ice	Elmer/Ice	Elmer/Ice	Elmer/Ice
Ocean component	ROMS	FVCOM	ROMS	FVCOM
Ice mesh	Unstructured	Semi-structured	Unstructured	Semi-structured
Ocean mesh or grid	Structured, staggered	Semi-structured	Structured, staggered	Semi-structured
Domain size	$30\,\mathrm{km} \times 100\,\mathrm{km}$	$31\,\mathrm{km} \times 99\,\mathrm{km}$	$30\,\mathrm{km} \times 100\,\mathrm{km}$	$31\,\mathrm{km} \times 99\,\mathrm{km}$
Regrid method	Bilinear	Nearest STOD	Bilinear	Nearest STOD
Ocean time-step	200 s	20 s	100 s	20 s
Ice time-step	10 days	10 days	10 days	10 days
Coupling interval	10 days	10 days	10 days	10 days
Run length	100 a	47 a	46 a	40 a
Cavity update method	**Rate**	**Rate**	**Corrected rate**	**Rate**
Cavity correction factor, f_{cav}	n/a	n/a	0.01	n/a
Minimum water column D_{crit}	n/a	n/a	5m	5m
Ocean density ρ_{or}	$1027\,\mathrm{kg\,m^{-3}}$	$1027.9\,\mathrm{kg\,m^{-3}}$	$1027\,\mathrm{kg\,m^{-3}}$	$1027.9\,\mathrm{kg\,m^{-3}}$
Ice density ρ_i	$910\,\mathrm{kg\,m^{-3}}$	$910\,\mathrm{kg\,m^{-3}}$	$910\,\mathrm{kg\,m^{-3}}$	$910\,\mathrm{kg\,m^{-3}}$
Ice temperature	$-5\,°\mathrm{C}$	$-5\,°\mathrm{C}$	$-5\,°\mathrm{C}$	$-5\,°\mathrm{C}$

passes an ice shelf basal melt rate to the ice component and the ice component passes a rate of change of ice draft to the ocean component.

275   We expect adjustment toward a uniform thickness ice shelf to occur by two mechanisms:

1. Ice dynamics. The gravitational driving force will tend to cause flow from thicker to thinner regions.

2. Melt/freeze. The greater pressures at greater depth should result in higher melt rates, with the potential for refreezing under thinner regions.

3.1.1   Domain size and meshes

280   The domain is 30 km across the expected direction of ice flow (y direction) by 100 km along the flow (x direction) for simulation VE1_ER. However, ocean component FVCOM (used in VE1_EF) uses a semi-structured (in principal structured but in practice exhibiting some structure) mesh with dimensions 31 km by 99 km. FISOC does not in general require that ice

and ocean component domains precisely overlap. Indeed the region of overlap is allowed to be small relative to the domains
(for example an Antarctic ice stream interacts with the ocean only in its floating shelf, and the majority of the catchment may
285 be grounded with no possibility to interact with the ocean for the duration of an intended simulation). However, given that we
aim to address mass conservation in the coupled system we choose to require precise domain match between ice and ocean
components for the current study. Therefore the ice component for VE1_EF runs on an almost identical mesh to the ocean
component. The only difference is at two diametrically opposite corners where FVCOM prefers to maintain element shape but
Elmer/Ice prefers to maintain a strictly rectangular domain (in order to facilitate imposition of consistent boundary conditions
290 at the corners of the domain). These mesh differences are visually summarised in Figure 2.

3.1.2 Ice component setup

The initial geometry is of an ice shelf at floatation (i.e. hydrostatic equilibrium). The initial ice draft is given in m by

$$D = -450 + 400 \left(\frac{x}{100000} \right), \tag{8}$$

where x is distance in m along the domain. The initial geometry does not vary across the ice flow (y direction). Ice and ocean
295 water densities used in the ice component are $\rho_i = 910 \ \mathrm{kg \, m^{-3}}$ and $\rho_{or} = 1027 \ \mathrm{kg \, m^{-3}}$ respectively. These densities, along
with the floatation assumption, determine the ice upper surface.

The pressure, P, acting on the underside of the ice shelf is given by

$$P(z) = -\rho_{or} g D. \tag{9}$$

where z is height relative to sea level (positive upward) and g is gravitational acceleration (set to $9.81 \ \mathrm{m \, s^{-2}}$).
300 Temperature in the ice component is constant through space and time at $-5 \ °C$.

VE1 includes ice flow and geometry evolution solving the Stokes equations directly. Glen's power law rheology with $n = 3$
is implemented (Glen, 1952; Gagliardini et al., 2013).

Zero net accumulation is prescribed at the upper ice surface. The melt rate from the ocean component is applied at the lower
surface. Flow through the vertical side boundaries is not allowed.
305 **Elmer/Ice specific details.** The Stokes equations are solved within Elmer/Ice (Gagliardini et al., 2013). A 2D horizontal
mesh of triangles with an approximate element size of 1km (VE1_ER) or 2km (VE1_EF) is extruded in the vertical to give 11
equally spaced terrain-following layers with the bulk element shape being triangular prisms.

3.1.3 Ocean component setup

The ocean bathymetry is set to $500 \ \mathrm{m}$ throughout the domain. The wet/dry scheme (Section 2.8) is not used in this experiment
310 as the whole domain is ice shelf cavity with no grounded ice. Boundaries are closed and rotation is disabled. Temperature
is initialised at $-1.85 \ °C$ and salinity at $34.6 \ \mathrm{psu}$. Ice-ocean thermodynamics are captured by means of the three-equation
parameterisation (Section 2.6).

Ice model mesh for ER simulations
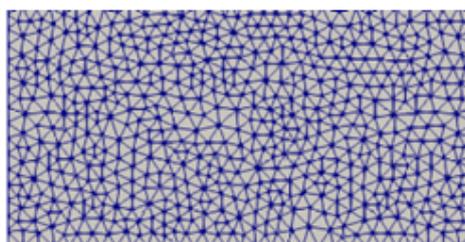
Ice model mesh for EF simulations
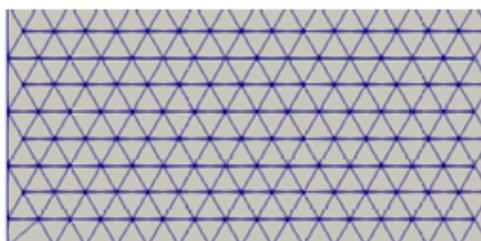
Ocean model mesh for EF simulations
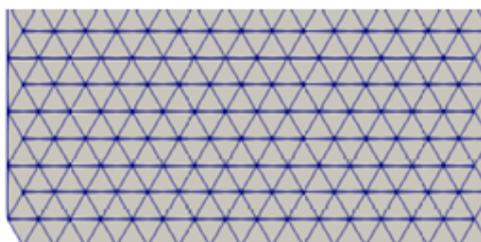
Figure 2. Unstructured meshes used in the current study. The first 15 km are shown. The ocean model in the ER simulations uses a structured grid.

The ocean conditions are chosen to represent a cold cavity ice shelf, such as the Amery Ice Shelf. In this configuration, both basal melting and refreezing can occur.

315   **ROMS specific details.** The horizontal resolution is a constant 1 km. There are 11 vertical layers, with a sigmoidal terrain-following distribution configured to provide increased resolution near the top and bottom surfaces. The ROMS baroclinic (slow) time-step is 200 seconds, and there are 30 barotropic (fast) time-steps for every slow time-step.

FVCOM specific details. The horizontal grid resolution is 2 km (defined by the distance between adjacent nodes within a uniform triangular grid) and there are 11 uniformly spaced vertical terrain-following layers. Interior vertical mixing is pa-

320 rameterized using the Mellor and Yamada level 2.5 (Mellor and Yamada, 1982) turbulent closure model (vertical Prandtl Number = 0.1) together with a constant background viscosity and diffusivity of 10^{-6} m^{2}s^{-1}. An eddy closure parameterisation (Smagorinsky, 1963) is used for the horizontal mixing of momentum (viscosity) and tracers (diffusivity) with both the scaling factor and the Prandtl Number being 0.1.

3.1.4 Coupling

325 The coupling interval is 10 days, the same as the ice component time-step. Cavity update method is **Rate** (Section 2.5). For VE1_ER the regridding method is bilinear with nearest STOD extrapolation for ocean cells that lie outside the ice domain due to grid stagger. For VE1_EF nearest STOD regridding is used, which results in a one to one mapping between ice and ocean nodes due to the meshes being nearly identical (Section 3.1.1). There is no grounding line in this experiment.

3.2 Verification experiment 2: grounding line evolution

330 Verification experiment 2 (VE2) is a modified version of VE1, but with part of the region grounded and a net ice flow through the domain allowed. The setup is identical to VE1 except where stated otherwise in this section.

3.2.1 Ice component setup

The VE2 initial geometry is given by

$$
\begin{aligned}
z_b &= -20 - 980\left(\frac{x}{100000}\right), & (10)\\
H &= \frac{\rho_{or}}{\rho_i}\left(470 - 400\left(\frac{x}{100000}\right)\right), & (11)
\end{aligned}
$$

where z_b is bedrock elevation relative to sea level and H is ice thickness. Then D and S are calculated based on floatation and the same densities as in VE1.

No restrictions to ice flow are imposed at the upstream and down stream boundaries given by $x = 0$ and either $x = 100$ km (for VE2_ER) or $x = 99$ km (for VE2_EF). Zero normal velocity and free slip tangential velocity conditions are imposed at

340 the side walls given by $y = 30$ km and either $y = 0$ (for VE2_ER) $y = -1$ km (for VE2_EF).

The grounding line is allowed to evolve solving a contact problem (Gagliardini et al., 2013).

A sliding relation with a simple effective pressure dependency is used under the grounded ice (Budd et al., 1979, 1984; Gladstone et al., 2017),

$$
\tau_b = -Cu_b^m z_*, \tag{12}
$$

345 where τ_b is basal shear stress, u_b is basal ice velocity, z_* is the height above buoyancy (related to effective pressure at the bed, N, by $N = \rho_i g z_*$), m is a constant exponent (set to $m = \frac{1}{3}$), and C is a constant sliding coefficient (set to C = 10^{-4} MPa m$^{-\frac{4}{3}}$ a$^{\frac{1}{3}}$).

Height above buoyancy is calculated by:

$$z_* = \begin{cases} H, & \text{if } D >= 0 \\ H - D\frac{\rho_{or}}{\rho_i}. & \text{if } D < 0 \end{cases} \tag{13}$$

350 This is equivalent to assuming a sub-glacial hydrology system fully connected to, and in pressure balance with, the ocean.

3.2.2 Ocean component setup

Ocean bathymetry matches the bedrock prescribed in the ice component (Equation 10). The wet/dry scheme (Section 2.8) is used in this experiment, with a critical water column thickness of $D_{crit} = 5$ m. Temperature is initialised at -1.9 °C and salinity at 34.6 psu.

355 **ROMS specific details.** The horizontal resolution is a constant 1 km. The slow time-step is 100 seconds, with 30 fast time-steps for every slow time-step. ROMS has 11 layers in the vertical.

FVCOM specific details. The FVCOM model setup is identical to that of Verification Experiment 1.

3.2.3 Coupling

The cavity update method for VE2_EF is **Rate** (Section 2.5). For VE2_ER it is **Corrected Rate** with a correction factor of
360 $f_{cav} = 0.01$. With the 10 day coupling interval this equates to a full correction timescale of approximately 3 years. Other coupling details are as in VE1.

4 Verification experiment results

4.1 VE1: Floating adjustment

This is a floating only experiment in which ice and ocean components adjust together towards an equilibrium state (described
365 in Section 3.1). We do not run long enough to achieve equilibrium, but instead investigate the conservation of mass in the coupled system as it evolves.

Figure 3 summarises the coupled system state at the start and end of simulation VE1_ER (see also Table 2 for a summary of the experiments). After the first coupling interval (10 days) the ocean component demonstrates a vigorous overturning circulation and high melt rates, especially in the deeper part of the domain. After the last coupling interval (100 years) the
370 combination of melting and ice flow has caused a redistribution of the ice shelf, with an overall reduction in the along-domain gradients. The melt rates and overturning circulation are much weaker than at the start.

The ocean circulation throughout the simulation is predominantly a buoyancy driven overturning along the domain, with very little cross-domain flow. The peak ocean flow speeds are always located at the top of the ocean domain directly under the ice shelf, where a fast, shallow buoyancy driven flow from deeper to shallower ice draft is balanced by a much deeper return
375 flow.
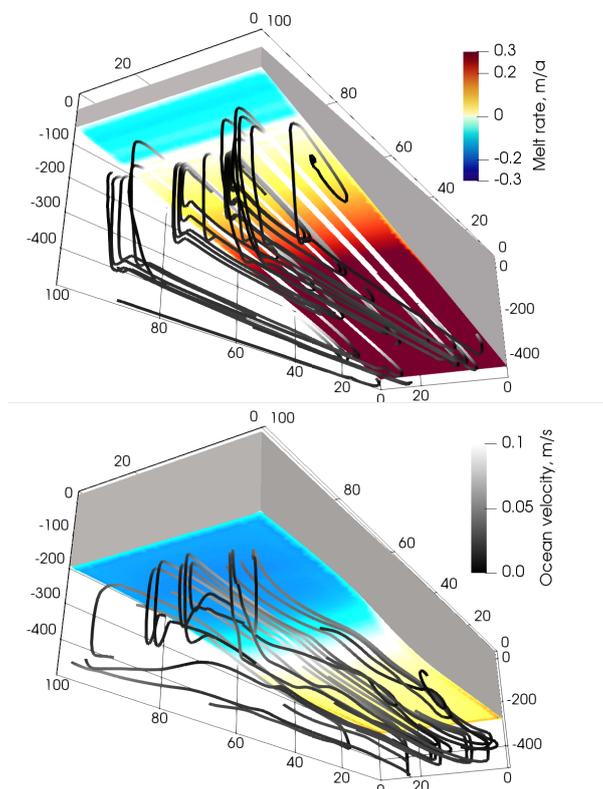
Figure 3. Coupled system state after the first (top) and last (bottom) coupling intervals from the experiment VE1_ER (Table 2). The ice shelf is shown in grey, with basal melt rate computed by the ocean shown in colour on the underside of the ice shelf. Ocean streamlines are shown beneath the ice shelf with the grayscale indicating magnitude of simulated ocean velocity. The vertical coordinate is given in m; the horizontal coords are given in km. This was a 100 year simulation.

Figure 4 shows the evolution over time of the total mass of both ice and ocean components and the total coupled system from experiments VE1_ER and VE1_EF. Relatively rapid mass transfer from the ice to the ocean occurs during the first few years as the relatively warm ocean water transfers its energy to the ice. After this initial period of net melting the ocean water temperature is close to freezing point, and a long term freezing trend can be seen, stronger and more sustained in the ROMS

380 ocean component than FVCOM. In a physically realistic coupled system the ice and ocean would come into thermodynamic equilibrium and the spatial net mass transfer would approach zero.

The net mass change of the coupled system is more than an order of magnitude smaller than the mass change of the individual components for both experiments VE1_ER and VE1_EF.
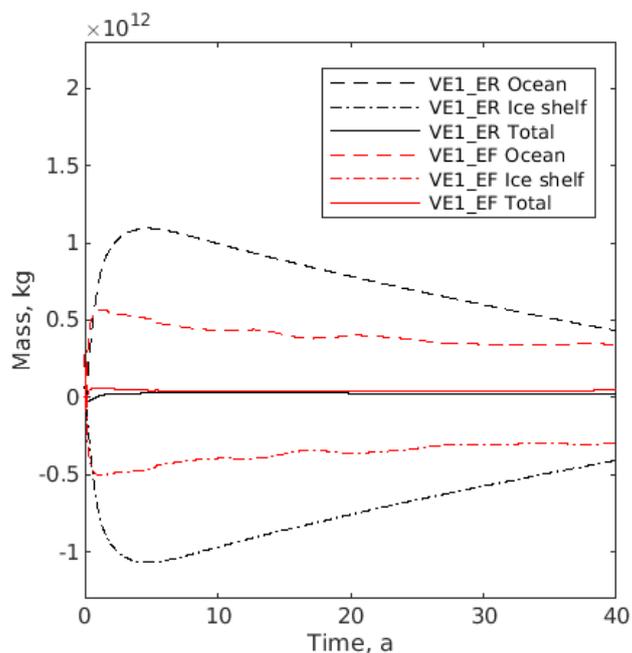
Figure 4. Simulated mass evolution over time for the ocean component (dashed lines), the ice component (dash/dot lines) and the total across both components (solid lines) from experiments VE1_ER (black) and VE1_EF (red).

4.2 VE2: grounding line evolution

385   This is a partially grounded experiment in which the ice component boundaries are not closed, a through-domain flow of ice is allowed, and the grounding line is allowed to evolve in the coupled system (described in Section 3.2). While the initial slope of the lower surface of the ice shelf is the same in both VE1 and VE2, the open inflow and outflow boundaries in the ice component, and the relatively shallower ice in the grounded region, both lead to a shelf that is much shallower in slope for VE2 than for VE1 for most of the simulation period. Figure 5 illustrates the shape of the ice sheet/shelf after 25 years from

390   simulation VE2_ER. The ice draft is deepest in the middle of the domain, at around 30km downstream (in terms of ice flow direction) from the grounding line. The ice draft impacts on circulation and melt, with the strong overturning of VE1_ER not present here. Melting occurs under the deepest ice, with refreezing elsewhere (Figure 6).

    Comparing the coupled simulation VE2_ER to the ice-only simulation (not shown) where the only difference is that the ice component features zero basal melt, it might be expected that the coupled simulation would exhibit a significantly thinner ice

395   shelf due to melting. However, the ice dynamics partially compensate for this in terms of the ice geometry: the melt-induced thinning leads to acceleration in the ice and the thickness difference is smaller than expected. However, this should not be interpreted as a stabilising feedback response of ice dynamics to ocean induced melting as the increased ice flow would tend to
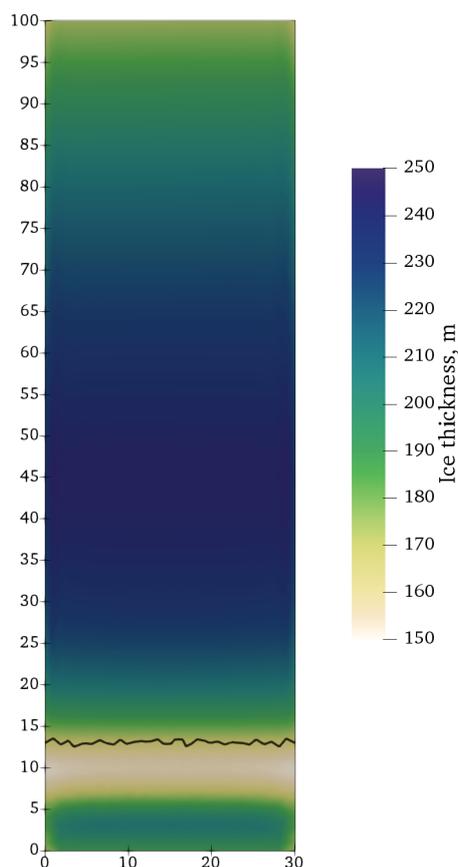
Figure 5. Plan view of the ice sheet thickness after 25 years of simulation VE2_ER. The black contour indicates the ISM grounding line position. Distances are given in km.

drain the grounded ice more quickly, potentially triggering marine ice sheet instability (Schoof, 2007). Instead this effect may tend to partially mask an ocean-induced ice sheet destabilisation if the observational focus is on ice shelf geometry.

400   As described in Section 2.8 the ice and ocean component each evolve the grounding line on their own time-step and on their own grid or mesh. There is potential for discrepancy between ice and ocean grounded area due to method of cavity evolution (Section 2.5), regridding errors, the inherent differences between grids or meshes, and the methods used to determine grounding line position. While ice geometry is a key determinant of grounding line position, the ice component also tests for a contact force (Gagliardini et al., 2013) and the ocean component ROMS tests height above buoyancy against the free surface variable 405 η (Section 2.8). Here we look at consistency of grounded area between components.
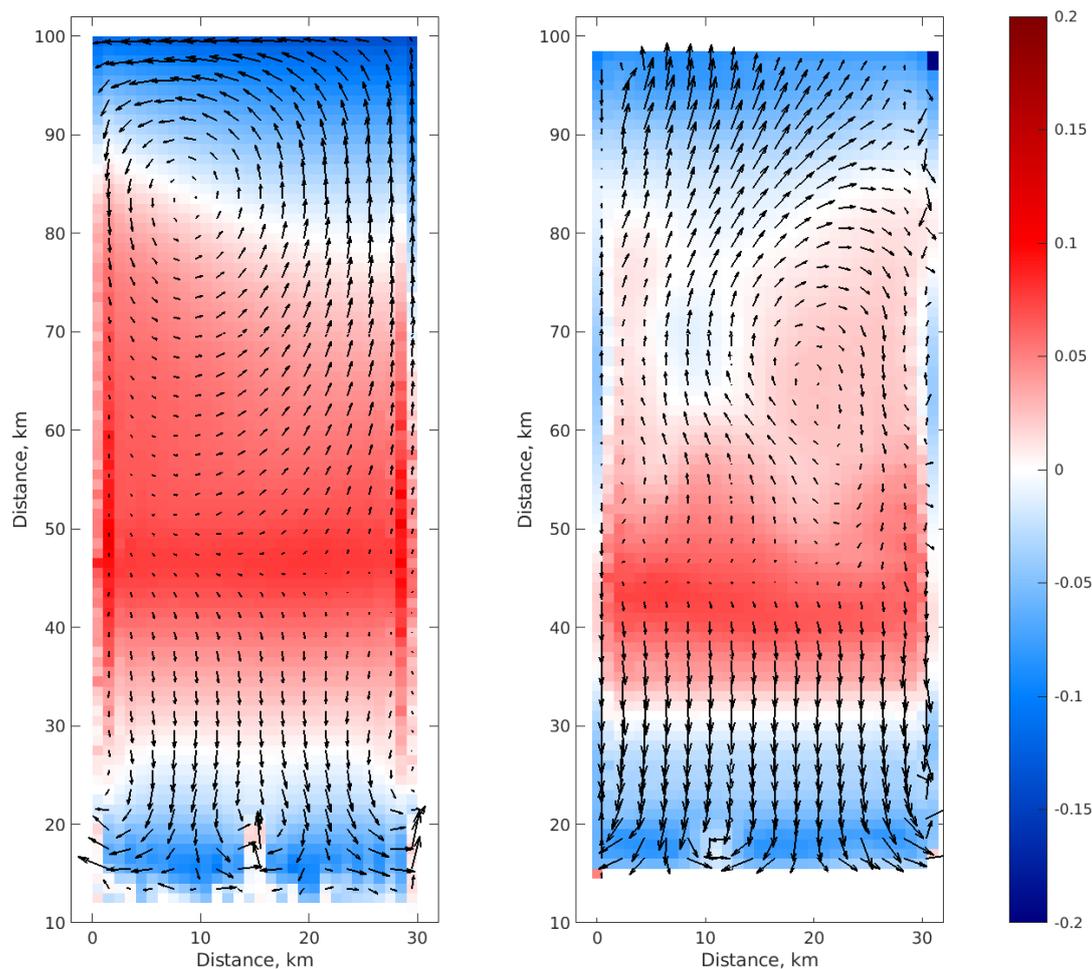
Figure 6. Ocean horizontal velocities in the upper layer (black arrows) and basal melt rate (red indicates melting, blue refreezing) after 25 years of simulation VE2_ER (left) and VE2_EF (right).

The evolution of grounded area in both ice and ocean components is shown in Figure 7 for simulation VE2_ER. While the ice component employs an unstructured mesh of triangular elements (on the lower surface of the 3D ice body), the ocean component employs a regular grid of square cells. The ocean component appears to exhibit a step-like reduction over time of grounded area. This is due to the row-by-row manifestation of grounding line retreat in the ocean component due to the alignment of grid rows with the linear downsloping geometry. Grounding line retreat starts at the lateral edges of a row (ungrounding near the sidewall boundary) and the "wetting" of dry cells propagates toward the centre of the row. This step-like
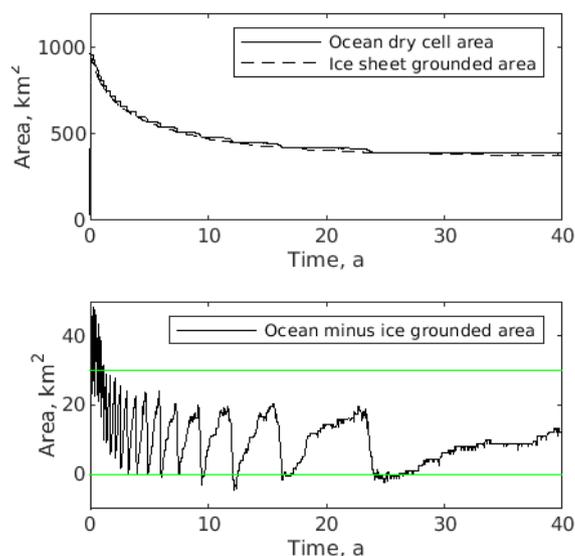
Figure 7. Top: A comparison of grounded area in the ocean component (total area of dry cells) against grounded area in the ice component (total area of grounded elements). Bottom: The difference between ocean and ice grounded area. These are from simulation VE2_ER. The green lines are drawn such that their distance apart is equivalent to the area of one row of ocean grid cells.

behaviour (with the spacing of the green lines in Figure 7 indicating the total area of a row of cells) explains the main difference between ice and ocean grounded area. The evolution of grounded area is shown in Figure 8 for simulation VE2_EF. Behaviour is similar to VE2_ER.

415   The initial rapid reduction in grounded area is due to the initial geometry. A region immediately upstream of the grounding line is initially very lightly grounded, and this region quickly becomes floating. The ocean component lags the ice component in this un-grounding, as can be seen in the first part of the difference plot in Figures 7 and 8. This lag is in part due to the "**Rate**" and "**Corrected rate**" cavity update methods, in which the ocean component uses the most recent two ice component outputs to calculate a rate of change of geometry. This inevitably causes the ocean component to lag by approximately one

420   coupling interval. The discrepancy may also be in part due to the fact that the region in question is close to floatation, thus the threshold for dry cells to become wet is highly sensitive to η, at least for the ROMS implementation.

The computational time spent in both the ice and ocean components was measured for simulation VE2_ER. The ice component is more expensive than the ocean component during the first coupling interval, but is significantly cheaper thereafter. Total time spent in the ice component over the 46 year simulation is approximately one third that spent in the ocean component.

425   The computational time spent within the central coupling code (calling routines and regridding) was negligible compared to time spent in ice and ocean components. This is with a 10 day coupling interval. If fully synchronous coupling is approached (i.e. if the coupling time-step approaches the ocean time-step) the ice component will become much more expensive and it
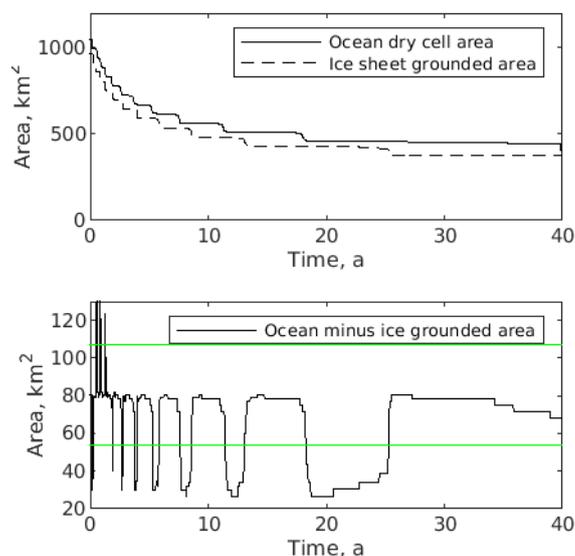
Figure 8. Top: A comparison of grounded area in the ocean component (total area of dry elements) against grounded area in the ice component (total area of grounded elements). Bottom: The difference between ocean and ice grounded area. These are from simulation VE2_EF. The green lines are drawn such that their distance apart is equivalent to the area of one row of ocean elements.

is possible the central coupling code may become significant. We do not anticipate fully synchronous ice-ocean coupling to become practical in the near future, at least not if the ice component directly solves the Stokes equations without simplifying assumptions, as is the case in the current study. The fully synchronous coupling of Goldberg et al. (2018); Snow et al. (2017) is achieved by using the "shallow shelf approximation" for the ice component and running both components on the same grid.

5 Conclusions

We have presented a flexible coupling framework for ice sheet/shelf and ocean models which allows the user to choose between different ice and ocean components. We have demonstrated the functioning of this framework in simple test cases, both with and without a moving grounding line. We have demonstrated conservation of mass and consistency of grounding line evolution using semi-synchronous coupling.

FISOC provides run time variable exchange on the underside of ice shelves. Providing such variable exchange at vertical ice cliffs, which are more common in Greenland than in Antarctica, will require minor developments to the coupling code, but the ocean components currently coupled through FISOC may need more significant developments in order to represent the buoyant plumes rising up ice cliffs.

Our coupled modelling framework is suitable for studying Antarctic ice sheet/shelf – ocean interactions at scales ranging from investigations of ice shelf channels (features with a spatial scale of typically a few km) up to whole Southern Ocean - Antarctic Ice Sheet coupled evolution. We are currently setting up simulations across this range of scales to address key processes surrounding Antarctic Ice Sheet stability and sea level contribution.

445 *Code availability.* The coupled modelling code is available from the FISOC github website https://github.com/RupertGladstone/FISOC under the GPL2 licence. The exact version of the FISOC code used to produce the results used in this paper, along with exact versions of ice and ocean model components, is given by code urls and specific commit hashes in a README file. This README file is archived along with the required input files on Finnish HPC machine Allas, and is publicly available from the Allas website https://a3s.fi/COLD_share/ FISOC_GMD_files.tar.gz.

450 *Author contributions.* RG led development, implementation of experiments, and paper writing. BGF, DG, QZ, TH, DS, SM, CZ, LJ, XG, KP, TZ contributed to development and or testing. BGF, DG, QZ, TH, CZ, YX, TZ contributed to implementation of experiments. All authors contributed to paper writing.

Competing interests. No competing interests are present.

Acknowledgements. Rupert Gladstone was funded from the European Union Seventh Framework Programme (FP7/2007-2013) under grant
455 agreement number 299035. This research was supported by Academy of Finland grants 286587 and 322430. The authors wish to acknowledge CSC - IT Centre for Science, Finland for computational resources. Tore Hattermann acknowledges financial support from Norwegian Research Council project 280727. Qin Zhou acknowledges financial support from Norwegian Research Council project 267660. Konstantinos Petrakopoulos's work was supported by CSLC grant G1204 from NYU Abu Dhabi.

References

460 Asay-Davis, X. S., Cornford, S. L., Durand, G., Galton-Fenzi, B. K., Gladstone, R. M., Gudmundsson, G. H., Hattermann, T., Holland, D. M., Holland, D., Holland, P. R., Martin, D. F., Mathiot, P., Pattyn, F., and Seroussi, H.: Experimental design for three interrelated marine ice sheet and ocean model intercomparison projects: MISMIP v. 3 (MISMIP+), ISOMIP v. 2 (ISOMIP+) and MISOMIP v. 1 (MISOMIP1), Geoscientific Model Development, 9, 2471–2497, https://doi.org/10.5194/gmd-9-2471-2016, http://www.geosci-model-dev.net/9/2471/ 2016/, 2016.

465 Budd, W., Keage, P. L., and Blundy, N. A.: Empirical studies of ice sliding, Journal of Glaciology, 23, 157–170, 1979.

Budd, W., Jenssen, D., and Smith, I.: A 3-dimensional time-dependent model of the West Antarctic Ice-Sheet, Annals of Glaciology, 5, 29–36, https://doi.org/10.3189/1984AoG5-1-29-36, 1984.

Chen, C., Liu, H., and Beardsley, R. C.: An unstructured grid, finite-volume, three-dimensional, primitive equation ocean model: Application to coastal ocean and estuaries, Journal of Atmospheric and Oceanic Technology, 20, 159–186, 2003.

470 Christianson, K., Bushuk, M., Dutrieux, P., Parizek, B. R., Joughin, I. R., Alley, R. B., Shean, D. E., Abrahamsen, E. P., Anandakrishnan, S., Heywood, K. J., Kim, T.-W., Lee, S. H., Nicholls, K., Stanton, T., Truffer, M., Webber, B. G. M., Jenkins, A., Jacobs, S., Bindschadler, R., and Holland, D. M.: Sensitivity of Pine Island Glacier to observed ocean forcing, Geophysical Research Letters, 43, 10,817–10,825, https://doi.org/10.1002/2016GL070500, https://agupubs.onlinelibrary.wiley.com/doi/abs/10.1002/2016GL070500, 2016.

Church, J., Clark, P., Cazenave, A., Gregory, J., Jevrejeva, S., Levermann, A., Merrifield, M., Milne, G., Nerem, R., Nunn, P., Payne, A.,
475 Pfeffer, W., Stammer, D., and Unnikrishnan, A.: Sea Level Change, in: Climate Change 2013: The Physical Science Basis. Contribution of Working Group I to the Fifth Assessment Report of the Intergovernmental Panel on Climate Change, edited by Stocker, T., Qin, D., Plattner, G.-K., Tignor, M., Allen, S., Boschung, J., Nauels, A., Xia, Y., Bex, V., and Midgley, P., Cambridge University Press, Cambridge, United Kingdom and New York, NY, USA, 2013.

Collins, N., Theurich, G., DeLuca, C., Suarez, M., Trayanov, A., Balaji, V., Li, P., Yang, W., Hill, C., and da Silva, A.: Design and Implemen-
480 tation of Components in the Earth System Modeling Framework, The International Journal of High Performance Computing Applications, 19, 341–350, https://doi.org/10.1177/1094342005056120, https://doi.org/10.1177/1094342005056120, 2005.

Cornford, S. L., Martin, D. F., Graves, D. T., Ranken, D. F., Le Brocq, A. M., Gladstone, R. M., Payne, A. J., Ng, E., and Lipscomb, W. H.: Adaptive mesh, finite volume modeling of marine ice sheets, Journal of Computational Physics, 232, 529–549, https://doi.org/10.1016/j.jcp.2012.08.037, 2013.

485 De Rydt, J. and Gudmundsson, G. H.: Coupled ice shelf-ocean modeling and complex grounding line retreat from a seabed ridge, Journal of Geophysical Research: Earth Surface, 121, 865–880, https://doi.org/10.1002/2015JF003791, https://agupubs.onlinelibrary.wiley.com/doi/abs/10.1002/2015JF003791, 2016.

Dinniman, M. S., Klinck, J. M., and Smith Jr., W. O.: Influence of sea ice cover and icebergs on circulation and water mass formation in a numerical circulation model of the Ross Sea, Antarctica, Journal of Geophysical Research: Oceans, 112,
490 https://doi.org/10.1029/2006JC004036, https://agupubs.onlinelibrary.wiley.com/doi/abs/10.1029/2006JC004036, 2007.

Favier, L., Durand, G., Cornford, S. L., Gudmundsson, G. H., Gagliardini, O., Gillet-Chaulet, F., Zwinger, T., Payne, A. J., and Le Brocq, A. M.: Retreat of Pine Island Glacier controlled by marine ice-sheet instability, Nature Climate Change, 4, 117–121, https://doi.org/10.1038/NCLIMATE2094, 2014.

Favier, L., Jourdain, N. C., Jenkins, A., Merino, N., Durand, G., Gagliardini, O., Gillet-Chaulet, F., and Mathiot, P.: Assessment of sub-shelf
melting parameterisations using the ocean–ice-sheet coupled model NEMO(v3.6)–Elmer/Ice(v8.3), Geoscientific Model Development,
12, 2255–2283, https://doi.org/10.5194/gmd-12-2255-2019, https://www.geosci-model-dev.net/12/2255/2019/, 2019.

Gagliardini, O., Zwinger, T., Gillet-Chaulet, F., Durand, G., Favier, L., de Fleurian, B., Greve, R., Malinen, M., Martín, C., Råback, P.,
Ruokolainen, J., Sacchettini, M., Schäfer, M., Seddik, H., and Thies, J.: Capabilities and performance of Elmer/Ice, a new-generation ice
sheet model, Geoscientific Model Development, 6, 1299–1318, https://doi.org/10.5194/gmd-6-1299-2013, https://www.geosci-model-dev.
net/6/1299/2013/, 2013.

Galton-Fenzi, B. K., Hunter, J. R., Coleman, R., Marsland, S. J., and Warner, R. C.: Modeling the basal melting and marine ice accretion of
the Amery Ice Shelf, Journal of Geophysical Research: Oceans, 117, https://doi.org/10.1029/2012JC008214, https://agupubs.onlinelibrary.
wiley.com/doi/abs/10.1029/2012JC008214, 2012.

Gladstone, R., Lee, V., Vieli, A., and Payne, A.: Grounding Line Migration in an Adaptive Mesh Ice Sheet Model, Journal of Geophysical
Research-Earth Surface, 115, https://doi.org/10.1029/2009JF001615, 2010a.

Gladstone, R., Payne, A., and Cornford, S.: Parameterising the grounding line in flow-line ice sheet models, The Cryosphere, 4, 605–619,
https://doi.org/10.5194/tc-4-605-2010, 2010b.

Gladstone, R., Lee, V., Rougier, J., Payne, A. J., Hellmer, H., Le Brocq, A., Shepherd, A., Edwards, T. L., Gregory, J., and Cornford, S. L.:
Calibrated prediction of Pine Island Glacier retreat during the 21st and 22nd centuries with a coupled flowline model, Earth And Planetary
Science Letters, 333, 191–199, https://doi.org/10.1016/j.epsl.2012.04.022, 2012.

Gladstone, R. M., Warner, R. C., Galton-Fenzi, B. K., Gagliardini, O., Zwinger, T., and Greve, R.: Marine ice sheet model performance
depends on basal sliding physics and sub-shelf melting, The Cryosphere, 11, 319–329, https://doi.org/10.5194/tc-11-319-2017, http://
www.the-cryosphere.net/11/319/2017/, 2017.

Glen, J. W.: Experiments on the deformation of ice, Journal of Glaciology, 2, 111–114, 1952.

Goldberg, D., Snow, K., Holland, P., Jordan, J., Campin, J.-M., Heimbach, P., Arthern, R., and Jenkins, A.: Representing grounding line
migration in synchronous coupling between a marine ice sheet model and a z-coordinate ocean model, Ocean Modelling, 125, 45 –
60, https://doi.org/https://doi.org/10.1016/j.ocemod.2018.03.005, http://www.sciencedirect.com/science/article/pii/S1463500318301021,
2018.

Hellmer, H. and Olbers, D.: A two-dimensional model for the thermohaline circulation under an ice shelf, Antarctic Science, 1, 325–336,
https://doi.org/10.1017/S0954102089000490, 1989.

Hellmer, H. H., Kauker, F., Timmermann, R., Determann, J., and Rae, J.: Twenty-first-century warming of a large Antarctic ice-shelf cavity
by a redirected coastal current, Nature, 485, 225–228, https://doi.org/10.1038/nature11064, 2012.

Hill, C., DeLuca, C., Balaji, Suarez, M., and Silva, A. d.: The Architecture of the Earth System Modeling Framework, Computing in Science
& Engineering, 6, 18–28, https://doi.org/10.1109/MCISE.2004.1255817, https://aip.scitation.org/doi/abs/10.1109/MCISE.2004.1255817,
2004.

Holland, D. M. and Jenkins, A.: Modeling Thermodynamic Ice–Ocean Interactions at the Base of an Ice Shelf, Journal of Physical Oceanog-
raphy, 29, 1787–1800, https://doi.org/10.1175/1520-0485(1999)029<1787:MTIOIA>2.0.CO;2, https://doi.org/10.1175/1520-0485(1999)
029<1787:MTIOIA>2.0.CO;2, 1999.

Mellor, G. and Yamada, T.: Development of a turbulence closure model for geophysical fluid problem., Reviews of Geophysics and Space
Physics, 20, 851–875, 1982.

Mercer, J.: West Antarctic Ice Sheet and CO2 Greenhouse Effect - Threat of Disaster, Nature, 271, 321–325, 1978.

Moore, J. C., Grinsted, A., Zwinger, T., and Jevrejeva, S.: Semiempirical And Process-Based Global Sea Level Projections, Reviews Of Geophysics, 51, 484–522, https://doi.org/10.1002/rog.20015, 2013.

Mueller, R. D., Hattermann, T., Howard, S. L., and Padman, L.: Tidal influences on a future evolution of the Filchner–Ronne Ice Shelf cavity in the Weddell Sea, Antarctica, The Cryosphere, 12, 453–476, https://doi.org/10.5194/tc-12-453-2018, https://www.the-cryosphere.net/12/453/2018/, 2018.

Pattyn, F., Huyghe, A., De Brabander, S., and De Smedt, B.: Role of transition zones in marine ice sheet dynamics, Journal of Geophysical Research-Earth Surface, 111, https://doi.org/10.1029/2005JF000394, 2006.

Robel, A. A., Seroussi, H., and Roe, G. H.: Marine ice sheet instability amplifies and skews uncertainty in projections of future sea-level rise, Proceedings of the National Academy of Sciences, 116, 14 887–14 892, https://doi.org/10.1073/pnas.1904822116, https://www.pnas.org/content/116/30/14887, 2019.

Schoof, C.: Ice sheet grounding line dynamics: Steady states, stability, and hysteresis, Journal of Geophysical Research-Earth Surface, 112, https://doi.org/10.1029/2006JF000664, 2007.

Seroussi, H., Nakayama, Y., Larour, E., Menemenlis, D., Morlighem, M., Rignot, E., and Khazendar, A.: Continued retreat of Thwaites Glacier, West Antarctica, controlled by bed topography and ocean circulation, Geophysical Research Letters, 44, 6191–6199, https://doi.org/10.1002/2017GL072910, https://agupubs.onlinelibrary.wiley.com/doi/abs/10.1002/2017GL072910, 2017.

Shchepetkin, A. F. and McWilliams, J. C.: The regional oceanic modeling system (ROMS): a split-explicit, free-surface, topography-following-coordinate oceanic model, Ocean Modelling, 9, 347–404, https://doi.org/10.1016/j.ocemod.2004.08.002, 2005.

Smagorinsky, J.: General circulation experiments with the primitive equations,I. The basic experiment, Monthly Weather Review, 91, 1963.

Snow, K., N. Goldberg, D., R. Holland, P., R. Jordan, J., J. Arthern, R., and Jenkins, A.: The Response of Ice Sheets to Climate Variability: ICE-OCEAN RESPONSE TO VARIABILITY, Geophysical Research Letters, 44, 2017.

Thoma, M., Determann, J., Grosfeld, K., Goeller, S., and Hellmer, H. H.: Future sea-level rise due to projected ocean warming beneath the Filchner Ronne Ice Shelf: A coupled model study, Earth and Planetary Science Letters, 431, 217 – 224, https://doi.org/https://doi.org/10.1016/j.epsl.2015.09.013, http://www.sciencedirect.com/science/article/pii/S0012821X15005804, 2015.

Vieli, A. and Payne, A.: Assessing the ability of numerical ice sheet models to simulate grounding line migration, Journal of Geophysical Research-Earth Surface, 110, https://doi.org/10.1029/2004JF000202, 2005.

Warner, J. C., Defne, Z., Haas, K., and Arango, H. G.: A wetting and drying scheme for ROMS, Computers & Geosciences, 58, 54 – 61, https://doi.org/https://doi.org/10.1016/j.cageo.2013.05.004, 2013.

Zhou, Q. and Hattermann, T.: Modeling ice shelf cavities in the unstructured-grid, Finite Volume Community Ocean Model: Implementation and effects of resolving small-scale topography, Ocean Modelling, 146, 101 536, https://doi.org/https://doi.org/10.1016/j.ocemod.2019.101536, http://www.sciencedirect.com/science/article/pii/S1463500319301738, 2020.